Triple band perfect absorber based on the metal-dielectric multilayer structure with cross-shaped plasmonic nanohole arrays

F. HU, F. CHEN*, G. WAMG, S. NIU, C. HUANG
Institute of Quantum Optics and Information Photonics, School of Physics and Optoelectronic Engineering, Yangtze University, Jingzhou 434023, People's Republic of China

In this paper, to realize triple-band perfect absorption, we present a numerical study of plasmonic absorption based on a metal-dielectric multilayer structure. The structure consists of cross-shaped plasmonic nanohole arrays with a silicon substrate. Results show that three absorption peaks (733 nm, 877 nm and 1340 nm) with the absorption of 95.2%, 99.5%, and 99.2% have been achieved, respectively. The perfect absorption peaks are caused by the localized surface plasmon resonance, Fabry Perot resonance and resonance of SPPs in the nanohole. The effect of structural parameters on absorption and field distribution is presented to illustrate the absorption mechanism. Moreover, the proposed absorber shows excellent angle tolerance approaching ±60°. As for refractive index sensor, the sensitivity is 728 nm/RIU, 425 nm/RIU and 398 nm/RIU, respectively. The results will pave the way towards the design of a multiple band plasmonic perfect absorber, which may have potential application in plasmonic absorption switch, plasmonic sensors and modulators.

1. Introduction

Surface plasmons polaritons (SPPs), which are electromagnetic wave propagating along with the metal-dielectric interface, have attracted a lot of attention in the past decades [1-7]. SPPs have an important role in the nanophotonic devices, such as optical absorbers, optical waveguides and plasmonic sensors [8-12]. SPR can be categorized into two types, one is propagating surface plasmons (PSPs), the other is localized surface plasmons (LSPs). Plasmonic perfect absorbers based on PSPs or LSPs have been present in metallic nanostructures and metamaterial [13-16]. Metamaterials based perfect absorbers have attracted a lot of attention due to its excellent plasmonic properties such as near-perfect absorption, huge localized field enhancement and subwavelength scale light concentration [17]. Many metamaterial based perfect absorbers have been widely studied theoretically and experimentally, for example, Yi et al. reported a tunable triple-band near-infrared metamaterial absorber based on Au nano-cuboids array [18]. Li et al. theoretically investigated a tunable perfect absorber based on propagating and localized surface plasmons using metal-dielectric-metals tructure [19]. Wu et al. designed and studied a wide-angle double-band plasmonic absorber which consists of metal-dielectric-metal split square ring and square array [20]. To achieve near perfect absorption, metamaterial is engineered by

minimizing the reflection and eliminating the transmission. A lot of perfect absorbers with specific functions have been gradually proposed, such as wide or narrow angle-dependent, polarization-independent, wide or narrow band, easy tunable [21-23].

The plasmonic perfect absorber based on surface plasmons in many previous works usually utilizes metal-dielectric-metal (MDM) structure, utilizing the plasmonic trapping by localized surface plasmon resonance and Fabry-Perot resonance to create ultranarrow absorption spectrum. MDM-based perfect absorbers are usually exhibited by perfect impedance matching, which has been proposed by engineering the size, material and shape of the structure. Very recently, our group reported a tunable double band perfect absorber based on a gold metal-dielectric grating multilayer structure [24-25].

In this paper, combined localized surface plasmon resonance and Fabry Perot resonance, a double band perfect absorber in the visible and infrared regime is realized. The proposed plasmonic perfect absorber is a four-layered structure, which consists of a silver-dielectric-silver structure with cross-shaped nanohole array, a silicon substrate placed at the bottom. Simulation results show that three absorption peaks (733 nm, 877 nm and 1340 nm) with the absorption of 95.2%, 99.5%, and 99.2% have been achieved. In particular, the three absorption peaks of the proposed absorber can be tuned by adjusting the sizes of the structure. The proposed

structure possess several advantages, such as triple band perfect absorption, excellent angle tolerance and easy fabrication. The design of our work may have potential application in the perfect absorber, optical switching and refractive sensing in the infrared range.

2. Geometry and simulation method

The proposed metal-dielectric multilayer structure is schematically depicted in Fig. 1, it consists of a two-dimensional cross-shaped air nanohole array on the top of silver-dielectric-silver film, the above structure is sitting on a silicon substrate.
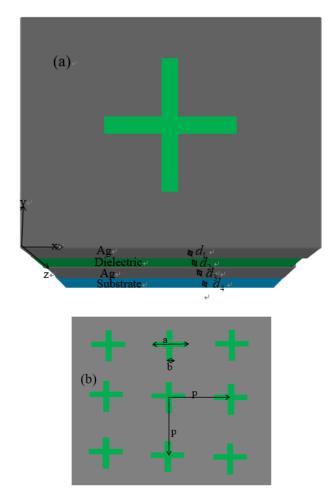

Fig. 1. (a) The schematic diagram of the proposed triple-band plasmonic perfect absorber composed of a multilayer ag-dielectric structure. (b) Top view of one unit of the proposed periodic structure

Where d_1, d_2, d_3 and d_4 are the thickness of the silver, dielectric, silver and silicon layer, the length and width of the proposed cross-shaped air nanohole are a and b. Fig. 1 b shows the top view of one unit of the proposed periodic structure, the period in x and y axis is p.

Three-dimensional finite-difference time-domain (FDTD) method is employed for the calculation of absorption properties of the proposed structure. In the simulation, a plane wave source with polarization along the x-direction is normally incident from Z direction, therefore the Perfect matched layers (PML) absorption boundary conditions are used in the Z direction. The wavelength of the incident plane wave is set to $\lambda=600\text{-}1600\ nm$, which covers the wavelength range of visible and infrared wave band. Due to the periodicity of the proposed structure, the simulation domain is made up of a single unit of the structure with periodicity boundary conditions along the x and y directions. The refractive index of dielectric layer is set to be 1.45 and the frequency-dependent complex relative permittivity of silver is characterized by the Drude model [26-27]:

$$\varepsilon(\omega) = 3.36174 - \frac{\omega_p^2}{\omega(\omega+i\omega_c)} \qquad (1)$$

where the plasma frequency of silver is $\omega_p=1.3388\times10^{16} rad/s$, and the damping constant is $\omega_c=7.07592\times10^{13}\ rad/s$ [28]. The refractive index of the silicon substrate is taken from Palik [29]. The reflection (R) and transmission (T) are calculated and then the absorption A is defined by A=1-T-R. In the paper the metal substrate is 150 nm, which is thick enough so the transmission can be approximately regarded as zero, therefore the absorption A can be calculated by A=1-R.

3. Simulation results

In the following simulation, the geometrical parameters are set as follows: the thickness of the top silver layer, dielectric layer, bottom silver layer and silicon substrate layer are set to be $d_1 = 50\,nm$, $d_2 = 40\,nm$, $d_3 = 150\,nm$, $d_4 = 800\,nm$. The period and size of the cross-shaped nanohole are $p = 500\ nm$, $a = 300\ nm$ and $b = 50\ nm$. It can be obtained that the transmission is negligibly small because the thickness of the bottom silver layer ($d_3 = 150\ nm$) is larger than the skin depth of light. The absorption spectra as a function of wavelength are calculated, and the results in the range of 600-1600 nm are shown in Fig. 2. It can be seen that the designed metal-dielectric multilayer absorber shows three absorption peaks (from left to right labeled by: mode 1, 733 nm, mode 2, 877 nm and mode 3, 1340 nm). And the absorptivity of the three peaks is 95.2%, 99.5%, and 99.2%, respectively, which indicates the proposed metal-dielectric multilayer structure can be used as triple-band plasmonic perfect absorber.
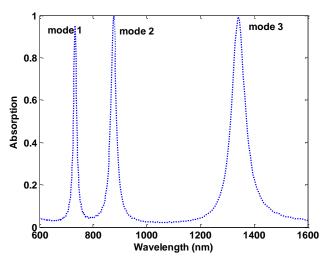
Fig. 2. The absorption spectrum of the proposed triple-band plasmonic perfect absorber calculated by FDTD. (The geometrical parameters were set as d_1=50 nm, d_2=40 nm, d_3=150 nm, d_4=800 nm, a=300 nm, b=50 nm, p=500 nm)

To reveal the physical absorption mechanism of the proposed metal-dielectric multilayer structure, the distributions of electric field ($|E_Z|^2$) of the absorption peaks ($\lambda_1=733\,nm$, $\lambda_2=877\,nm$ λ_2=877 nm, λ_3=1340 nm) and

absorption dip ($\lambda_4=1100\,nm$) are shown in Fig. 3 As can be seen from Fig. 3 (a) and (e), the absorption peak of wavelength is 611 nm, the electric field mainly distributes at the two ends of cross nanohole in the x-direction. Therefore mode 1 can be attributed to localized surface plasmon resonance of cross-shaped nanohole. From Fig. 3(b), the strong electric field mainly concentrated at the four corners of cross nanohole, and from Fig. 3(f), it can be seen that at the cross-section of the xz plane, electric field distributions strongly occur at the top and at the bottom surfaces of the cross-shaped nanohole, which indicates that mode 2 can be attributed to the resonance of SPPs in the nanohole. From Fig. 3(c), the strong electric field also concentrated at the four corners of cross nanohole, but from Fig. 3(g), it can be noticed that the strong electric field concentrated in the dielectric layer, which indicates that mode 3 can be attributed to the Fabry-Perot resonance effect of SPPs in the cross nanohole. Fig. 3(d) and (h) shows the steady-state electric field distribution of non-resonance wavelength $\lambda_4=1100\,nm$, in contrast to Fig. 3(a) and (e), the enhancement ($\sqrt{3.5}$ factors) is significantly lower than the field enhancement at resonance ($\sqrt{500}$ factors). Therefore the proposed triple-band perfect absorber is originated from different absorption mechanisms.
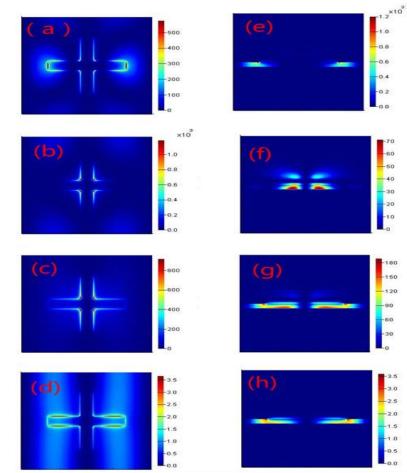

Fig. 3. Electric field $|E_Z|^2$ distribution of mode 1 (λ_1=733 nm), mode 2 (λ_2=877 nm), mode 3 (λ_3=1340 nm), off resonant wavelength (λ_4=1100 nm) (a)-(d) at xoy plane. (e)-(h) at xoz plane (color online)

In the following section, we will study the effect of structure parameters on the absorption characteristics. Fig. 4 illustrates the absorption spectra with different thicknesses of the top silver layer, the structure parameters are fixed. When the thickness of the silver layer d_1 is changed from 50 nm to 80 nm. The absorption peaks of mode 1 and mode 2 show a minor red-shift, but mode 3 shows a significantly blue-shift. This is because mode a and mode 2 are attributed to the localized surface plasmon resonance (LSP) of cross-shaped nanohole, the increase of d_1 will not affect the LSP. The maximum absorption values of the three modes remain perfect. The influence of dielectric layer thickness on the absorption spectra is then investigated. The results are shown in Fig. 5(a), where the other geometrical parameters are fixed unchanged, but the thickness of the dielectric layer is changed from 30 nm to 40 nm, 50 nm, 60 nm, and 70 nm respectively. One can see the resonant absorption peaks are blueshifted and the maximum absorption can be achieved when $d_2=40$ nm. As the thickness of the dielectric layer increases, the absorbance is becoming smaller and smaller. This phenomenon can be explained as follows, the dielectric layer will weaken the strength of light- matter interaction. Less energy will be confined in the dielectric layer. When the thickness of the dielectric layer $d_2=40$ nm, interaction between the SPPs at the upper and bottom interfaces of the dielectric layer leads to about 100% absorption efficiency. Therefore by design an appropriate nanostructure with parameter optimization, triple band perfect plasmonic absorption can be obtained. It can also be noticed that mode 3 is more sensitive to the variation of d_2, this is because mode 3 is originated from the Fabry-Perot resonance effect. Fig. 5(b) shows the absorption spectra with different periods p, one can see that when increasing the period, the absorption peaks exhibit a redshift. Given that mode 1 and mode 2 are attributed to LSP resonance of the cross nanohole, the increase of periods *p will increase the electron oscillation length of the silver film, resulting in the red shift of resonant mode*. Therefore, we can tune the absorption peak by adjusting the thickness of the silver layer, the dielectric layer and the periods of the proposed structure.
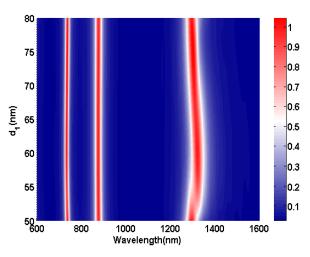

Fig. 4. The absorption spectra of the triple-band plasmonic perfect absorber with different thicknesses of top silver film d_1 (color online)
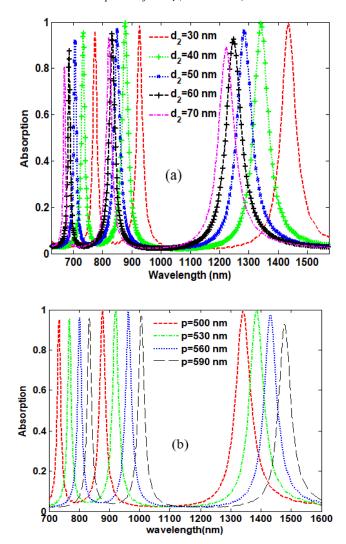

Fig. 5. The absorption spectra of the triple-band plasmonic perfect absorber with different parameters (a) thicknesses of dielectric layer d_2. (b) the period p (color online)

To investigate the effect of the size of the cross-shaped nanohole to the absorption spectra, we vary the length and width of the cross-shaped nanohole. Fig. 6(a) shows the absorption spectra with different (*a*), when the length of cross-shaped nanohole is changed from 280 nm to 300 nm, 320 nm, 340 nm, it can be noticed that the three absorption peaks undergo red shifts, and the position of mode 3 shifts more quickly than that of mode 1 and mode 2. And when the length of cross-shaped nanohole is *a=300 nm*, the maximum absorbance can be achieved, increasing the length of nanohole will increase the electron oscillation length of the top silver layer, resulting in the red shift of the absorption peak. Fig. 6(b) shows the influence of width of nanohole on the absorption spectra, when the width of nanohole is changed from 40 nm to 50 nm, 60 nm, the absorption peaks undergo blue shifts. This is because increasing the width of nanohole will reduce the gap between adjacent nanohole. According to the equivalent LC resonance circuit theory, the resonant frequency can be expressed as $f = 1/2\pi\sqrt{LC}$, the equivalent capacitance C will increase with the increase of the a and b, thus resulting in the blue shift of the resonance mode.

distribution in Fig. 3(g) indicates that the field located in the dielectric layer which is easy to interact with the surrounding medium, the refractive index sensitivity is expected to be high. To investigate the sensing performance of the proposed structure, the absorption spectra with different refractive indices from 1.25 to 1.55 are presented in Fig. 7(a). It reveals that a red shift of the absorption peaks with increasing the refractive index. Sensitivity and FOM are usually used to evaluate the sensing performance, the refractive index sensitivity of the proposed silver-dielectric multilayer structure is about 398 nm/RIU, 425 nm/RIU, 728 nm/ RIU for mode 1, mode 2 and mode 3, respectively. Fig. 7(b) shows the linear relationship between the resonance absorption peaks and the refractive indices *n*. Comparing with the sensing performance of other related structures, the sensitivity of our structure is the highest [30-31]. Therefore, the above results show that the proposed silve dielectric multilayer structure can be used for absorber and refractive index sensing in the visible or infrared region, which may be applied to the study of small molecular sensing and optical absorption switching [32-33].
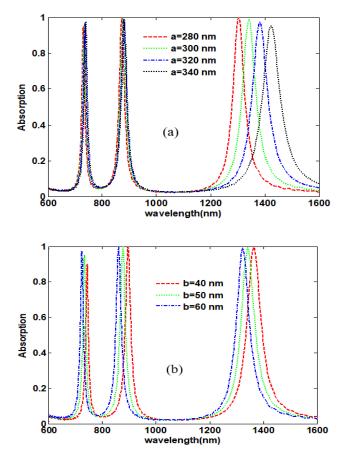

Fig. 6. The absorption spectra of the triple-band plasmonic perfect absorber with different values of cross air nanohole (a) The   length of cross air nanohole a (b) The width of cross air nanohole b (color online)
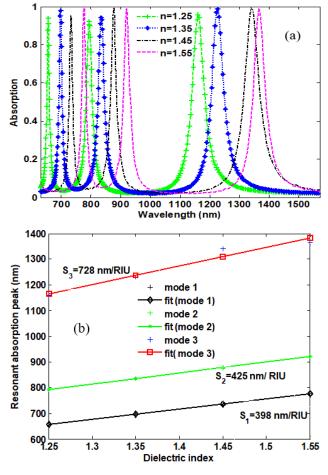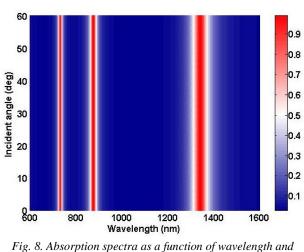

Fig. 7. (a) The transmission spectra of the triple-band plasmonic perfect absorber with changing dielectric refractive indices n from 1.25 to 1.55. (b) The linear relationship of the resonant   absirption peak versus the refractive indices n (color online)

Since the absorption spectra of the proposed metamaterial structure are very sharp, and the field

Fig. 8. Absorption spectra as a function of wavelength and incident angle (color online)

In practice, incident electromagnetic wave interacts with the plasmonic absorber with an oblique angle, the absorption spectra as a function of the incident angle are shown in Fig. 8, it can be seen that for the proposed absorber, the position of the absorption peak keeps unchanged over a wide-angle range of incidence about ±60°. It is because the proposed silver dielectric multilayer structure possesses good symmetry [34]. The proposed structure can be easily made by nanoimprint lithography which is believed to be applied in small molecular sensing and optical absorption switching in the visible or infrared region [35].

It is worth mentioning that our structure has better performance when compared with that of other similar plasmonic perfect absorbers [36-39]. As listed in Table 1, the performance of the absorber designed in this paper is excellent. The results show that the perfect wave absorbing device based on double elliptical and L-shaped graphene has more resonance bands, greater absorption efficiency and wider application prospects.

Tabel 1. The parameter's values obtained in this work compared with those of other similar plasmonic perfect absorbers (NM means not mentioned in the references)

Reference	This work	R36	R37	R38	R39
Resonance wavelength (nm)	733 877 1340	1456	750 1050	1247 1697	11600
Absorption (%)	95.2, 99.5, 99.2	99.9	99.89 99.59	99.5 99	99.5
angle tolerance	±60°	NM	NM	±50°	±60°
Sensitivity (nm/RIU)	728, 425, 398	405	800 1200	NM	NM
Tunability	Yes	Yes	Yes	Yes	Yes

4. Conclusions

In this paper, we investigate numerically a silver dielectric multilayer structure. Triple band ($\lambda_1=733$ nm, $\lambda_2=877$ nm, $\lambda_3=1340$ nm) perfect absorption (95.2%, 99.5%, and 99.2%) has been realized due to the localized surface plasmon resonance, Fabry Perot resonance and resonance of SPPs in the nanohole. The localized surface plasmon resonance, Fabry Perot resonance and resonance of SPPs in the nanohole. The absorption peak can be tuned by changing geometrical parameters such as silver layer and dielectric layer thickness, nanohole size period. Moreover, the proposed absorber shows excellent angle tolerance approaching ±60°. As for refractive index sensor, the sensitivity are 728 nm/RIU, 425 nm/RIU and 398 nm/RIU. Our research results may benefit a lot of applications, including plasmonic absorption switch, plasmonic modulator and refractive index sensor with high sensitivity.

References

[1] N. I. Landy, S. Sajuyigbe, J. J. Mock, D. R. Smith, W. J. Padilla, Phys. Rev. Lett. **100**, 207402 (2008).

[2] S. Kim, J. Jin, Y. J. Kim, I. Y. Park, Y. Kim, S. W. Kim, Nature **453**, 757 (2008).

[3] H. Chalabi, D. Schoen, M. L. Brongersma, Nano Lett. **14**, 1374 (2014).

[4] D. Dutta-Gupta, O. J. F. Martin, S. D. Gupta, G. S. Agarwal, Opt. Express **20**, 1330 (2012).

[5] J. Rosenberg, R. V. Shenoi, T. E. Vandervelde, S. Krishna, O. Painter, Appl. Phys. Lett. **95**, 161101 (2009).

[6] H. Wenbo, B. C. Stephen, Advanced Functional Materials **23**(13), 1612 (2013).

[7] Y. S. Zhu, H. X. Xu, Y. Peng, Z. M. Wang, Nano Lett. **8**, 021305 (2021).

[8] J. N. Anker, W. P. Hall, O. Lyandres, N. C. Shah, J. Zhao, R. P. Van Duyne, Nat. Mater. **7**, 442 (2008).

[9] Y. Wang, T. Sun, T. Paudel, Y. Zhang, Z. Ren, K. Kempa, Nano Lett. **12**, 440 (2012).

[10] M. Kang, F. Liu, T. F. Li, Q. H. Guo, J. Li, J. Chen, Opt. Lett. **38**, 3086 (2013).

[11] C. M. Watts, X. Liu, W. J. Padilla, Adv. Mater. **24**, 98 (2012).

[12] C. W. Cheng, M. N. Abdas, C. W. Chiu, K. T. Lai, M. H. Shih, Y. C. Chang, Opt. Express **20**, 10376 (2012).

[13] Z. H. Chen, H. Chen, H. G. Jile, D. Y. Xu, Z. Yi, Y. L. Lei, X. F. Chen, Z. G. Zhou, S. S. Cai, G. F. Li, Diamond and Related Materials **115**, 108374 (2021).

[14] Z. Liu, G. Liu, G. Fu, X. Liu, Y. Wang, Opt. Express **24**, 5020 (2016).

[15] S. W. Shu, Y. Y. Li, Opt. Lett. **37**, 3495 (2012).

[16] H. M. Lee, J. C. Wu, J. Phys. D: Appl. Phys. **45**, 205101 (2012).

[17] C. W. Cheng, M. N. Abdas, C. W. Chiu, K. T. Lai, M. H. Shih, Y. C. Chang, Opt. Express **20**, 10376 (2012).

[18] F. Qin, Z. Q. Chen, X. F. Chen, Z. Yi, W. T. Yao, T. Duan, P. H. Wu, H. Yang, G. F. Li, Y. G. Yi, Nanomaterial **10**, 5 (2020).

[19] Q. Li, J. S. Gao, H. G. Yang, H. Liu, X. Y. Wang, Z. Z. Li, X. Guo, Plasmonics **12**, 1037 (2017).

[20] H. M. Lee, J. C. Wu, J. Phys. D: Appl. Phys. **45**, 205101 (2012).

[21] Y. S. Zhai, G. D. Chen, J. Xu, Z. Y. Qi, X. H. Li, Q. L. Wang, Opt. Commun **399**, 28 (2017).

[22] M. B. Pu, C. G. Hu, M. Wang, C. Huang, Z. Y. Zhao, C. T. Wang, Q. Feng, X. G. Luo, Opt. Express **19**, 17413 (2011).

[23] B. X. Zhang, Y. H. Zhao, Q. Z. Hao, B. Kiraly, I. C. Khoo, S. F. Chen, T. J. Huang, Opt. Express **19**, 15211 (2011).

[24] L. Zhang, Y. Wang, L. Zhou, F. Chen, Appl. Phys. A **125**, 368 (2019).

[25] F. Chen, H. F. Zhang, L. H. Sun, J. J. Li, C. C. Yu, Appl. Phys. A **125**, 792 (2019).

[26] W. Wang, Z. H. Zhao, C. Guo, K. Guo, Z. Y. Guo, Nanomaterials **9**, 761 (2019).

[27] F. Chen, H. F. Zhang, L. H. Sun, J. J. Li, C. C. Yu, Opt. Laser. Technol. **116**, 293 (2019).

[28] C. Liu, G. L. Fu, F. M. Wang, Z. Yi, C. H. Xu, L. Yang, Q. Liu, W. Liu, X. L. Li, H. W. Mu, T. Sun, P. K. Chu, Optik **196**, 163173 (2019).

[29] C. L. Cen, Z. Yi, G. F. Zhang, Y. B. Zhang, C. P. Liang, X. F. Chen, Y. J. Tang, X. Ye, Y. G. Yi, J. Q. Wang, J. J. Hua, Results Phys. **14**, 102463 (2019).

[30] K. Q. Le, Q. M. Ngo, T. K. Nguyen, IEEE J. Sel. Top. Quantum Electron. **23**, 6900506 (2016).

[31] K. Q. Le, A. Alu, J. Bai, J. Appl. Phys **117**, 023118 (2015).

[32] X. Y. Lu, R. G. Wu, T. Y. Zhang, Opt. Express **23**, 29842 (2015).

[33] N. Liu, M. Mesch, T. Weiss, M. Hentschel, H. Giessen, Nano Letters **10**, 2342-8 (2010).

[34] Z. Q. Chen, P. Li, S. Zhang, Y. Q. Chen, P. Liu, H. G. Duan, Nanotechnology **30**, 335201 (2019).

[35] I. Hwang, M. Kim, J. Yu, J. Lee, J. H. Choi, S. A. Park, W. S. Chang, J. Lee, J. Y. Jung, Small Methods **5**, 2100277 (2021).

[36] X. Yin, T. Sang, H. L. Qi, G. Q. Li, X. Wang, J. C. Wang, Y. K. Wang, Scientific Reports **9**, 17477 (2019).

[37] Y. F. C. Chau, C. T. C. Chao, H. J. Huang, M. R. R. Kooh, N. T. R. N. Kumara, C. M. Lim, H. P. Chiang, Nanomaterials **10**, 493 (2020).

[38] B. X. Zhang, Y. H. Zhao, Q. Z. Hao, B. Kiraly, I. C. Khoo, S. F. Chen, T. J. Huang, Opt. Express **19**(16), 15221 (2011).

[39] H. J. Li, L. L. Wang, X. Zhai, Scientific Reports **6**, 36651 (2016).

---

*Corresponding author: 501110@yangtzeu.edu.cn